Published for SISSA by Springer

Received: March 3, 2021
Revised: September 9, 2021
Accepted: October 4, 2021
Published: October 21, 2021

JHEP10(2021)177

Observation of $e^+e^- \to \eta\psi(2S)$ at center-of-mass energies from 4.236 to 4.600 GeV

BESIII

The BESIII collaboration

E-mail: besiii-publications@ihep.ac.cn

Abstract: Using a total of 5.25 fb^{-1} of e^+e^- collision data with center-of-mass energies from 4.236 to 4.600 GeV, we report the first observation of the process $e^+e^- \to \eta\psi(2S)$ with a statistical significance of 4.9 standard deviations. The data sets were collected by the BESIII detector operating at the BEPCII storage ring. We measure the yield of events integrated over center-of-mass energies and also present the energy dependence of the measured cross section.

Keywords: e^+-e^- Experiments, Exotics, Particle and resonance production, Quarkonium

ArXiv ePrint: 2103.01480

https://doi.org/10.1007/JHEP10(2021)177

Contents

1 Introduction

The recent observation of a number of unexpected vector charmonium-like states ($J^{PC} = 1^{--}$) above open-charm threshold has stimulated theoretical and experimental studies of the conventional and exotic states in this energy region [1–7]. These vector states, originally called the $Y(4260)$ [8–12], the $Y(4360)$ [13–15], and the $Y(4660)$ [14, 15], observed by the BaBar, Belle, and CLEO experiments, can be produced via the initial state radiation (ISR) process, and are often observed in final states with two pions and a charmonium state, like the J/ψ or $\psi(2S)$. They differ from the $\psi(3770)$, $\psi(4040)$, $\psi(4160)$, and $\psi(4415)$ states which are observed in the e^+e^- inclusive hadronic cross section [16] and match potential model calculations of the charmonium spectrum [17]. The Y states have many theoretical interpretations, including compact tetraquarks, molecules, hybrids, hadrocharmonia [1–7], and so on, but they are still not well understood.

In recent years two resonant structures around 4.22 and 4.32 GeV/c^2 were observed in a fit to the cross section of $e^+e^- \to \pi^+\pi^- J/\psi$ measured by the BESIII experiment [18]. The lower mass structure, the $Y(4220)$, is interpreted as the main component of the well-known $Y(4260)$ structure [8–12], and the higher mass structure, the $Y(4320)$, could be the $Y(4360)$ resonance [13–15, 19] observed in the process $e^+e^- \to \pi^+\pi^-\psi(2S)$. A series of cross-section measurements of $e^+e^- \to \pi^+\pi^- h_c$ [20], $e^+e^- \to \omega\chi_{c0}$ [21], and $e^+e^- \to \pi^+ D^0 D^{*-}$ together with the charge-conjugate (*c.c.*) mode [22] has been reported by BESIII, and the parameters of the $Y(4220)$ resonance in these processes are consistent with those measured in the $e^+e^- \to \pi^+\pi^- J/\psi$ process [18].

JHEP10(2021)177

Searching for new decay modes of Y states produced in e^+e^- annihilation and measuring the line shapes of the production cross sections will shed light on the nature of the Y states. Besides the $\pi\pi$ hadronic transitions, other hadronic transitions (via η, η') of these Y states to lower mass charmonium states such as the J/ψ or $\psi(2S)$ also provide further insight into their internal structure. The CLEO-c [23], Belle [24], and BESIII [25–27] experiments measured the cross section of $e^+e^- \to \eta J/\psi$, and BESIII observed the decays $Y(4220) \to \eta J/\psi$ and $Y(4390) \to \eta J/\psi$ [27] for the first time. The authors of ref. [28] reproduced the measured $e^+e^- \to \eta J/\psi$ line shape and predicted the production cross section of the analogous process $e^+e^- \to \eta' J/\psi$ at $\mathcal{O}(\alpha_s^4)$ accuracy in the framework of non-relativistic Quantum Chromodynamics (NRQCD). However, the measured cross section of $e^+e^- \to \eta' J/\psi$ [29, 30] by BESIII is significantly smaller than the theoretical prediction [28].

To provide more information for the study of the vector charmonium-like states, the cross section of $e^+e^- \to \eta\psi(2S)$ can also be compared with those of the processes $e^+e^- \to \eta J/\psi$ and $e^+e^- \to \eta' J/\psi$. The CLEO-c experiment searched for the process $e^+e^- \to \eta\psi(2S)$ with data at center-of-mass (c.m.) energy $\sqrt{s} = 4.260\,\text{GeV}$, and reported an upper limit on the Born cross section, $\sigma[e^+e^- \to \eta\psi(2S)] < 25$ pb, at a 90% confidence level (C.L.) [23]. This is the only available experimental study of this process.

In this article, we present a study of $e^+e^- \to \eta\psi(2S)$ at 14 c.m. energies from 4.236 to 4.600 GeV, using data collected with the BESIII detector [31] operating at the BEPCII collider [32]. The total integrated luminosity is $5.25\,\text{fb}^{-1}$. The c.m. energies were measured using $e^+e^- \to \mu^+\mu^-$ events with an uncertainty of 0.8 MeV [33] and the integrated luminosities were measured using Bhabha scattering events to an uncertainty of 1.0% [34, 35]. The $\psi(2S)$ is reconstructed using the decay chain $\psi(2S) \to \pi^+\pi^- J/\psi$, $J/\psi \to \ell^+\ell^-$ ($\ell = e$, μ), and the η using $\eta \to \gamma\gamma$.

2 BESIII detector and Monte Carlo simulation

The cylindrical core of the BESIII detector consists of a helium-based multilayer drift chamber (MDC), a plastic scintillator time-of-flight system (TOF), and a CsI(Tl) electromagnetic calorimeter (EMC), which are all enclosed in a superconducting solenoidal magnet providing a 1.0 T magnetic field. The solenoid is supported by an octagonal flux-return yoke with resistive plate chamber muon identifier modules interleaved with steel. The acceptance of charged particles and photons is 93% over 4π solid angle. The charged-particle momentum resolution at 1 GeV/c is 0.5%, and the dE/dx resolution is 6% for the electrons from Bhabha scattering events. The EMC measures photon energies with a resolution of 2.5% (5%) at 1 GeV in the barrel (end cap) region. The time resolution of the TOF barrel part is 68 ps, while that of the end cap part is 110 ps. The end cap TOF system was upgraded in 2015 with multi-gap resistive plate chamber technology, providing a time resolution of 60 ps [36, 37].

To optimize the signal event selection criteria, estimate the background contributions and determine the detection efficiency, simulated samples are produced with the GEANT4-based [38] Monte Carlo (MC) package which includes the geometric description of the BESIII detector and the detector response. The signal MC events of $e^+e^- \to \eta\psi(2S)$ with

JHEP10(2021)177

the corresponding η and $\psi(2S)$ decay modes are generated using HELAMP and EVTGEN [39, 40] at each c.m. energy. The beam energy spread and ISR in the e^+e^- annihilations are modelled with the generator KKMC [41, 42] and the final state radiations (FSR) from charged final-state particles are incorporated with the PHOTOS package [43]. The possible background contributions are also studied with KKMC [41, 42] at each c.m. energy. The decay modes are modelled with EVTGEN using branching fractions taken from the PDG [16].

3 Event selection

Candidate events with four charged tracks with zero net charge and at least two photons are selected. The charged tracks are required to be well reconstructed in the MDC with a polar angle θ satisfying $|\cos\theta| < 0.93$; and their distances of the closest approach to the interaction point in $x-y$ plane and z direction have to be less than 1 cm and 10 cm, respectively. Since the $\pi^\pm$ and $\ell^\pm$ are kinematically well separated, charged particles with momenta less than 0.8 GeV/c in the laboratory frame are assumed to be $\pi^\pm$, whereas the ones with momenta larger than 1.0 GeV/c are assumed to be $\ell^\pm$. To separate electron from muon candidates, the EMC deposited energy is used. The energy deposits of electron candidates and muon candidates are required to be larger than 1.0 GeV and less than 0.4 GeV, respectively. Photon candidates are reconstructed from showers in EMC crystals. The reconstructed energies for the clusters in the barrel ($|\cos\theta| < 0.80$) and the end caps ($0.86 < |\cos\theta| < 0.92$) of the EMC are required to be higher than 25 and 50 MeV, respectively. To eliminate showers associated with charged particles, the angle between the photon and any charged track in the EMC must be at least 10 degrees. To suppress the electronic noise and energy deposits unrelated to the event, the time of the EMC shower is required to be $0 \leqslant t \leqslant 700$ ns with respect to the start of the event. To improve the mass resolution and suppress background contributions, we require charged tracks to originate from a common vertex. In addition, a four-constraint (4C) kinematic fit is performed under the hypothesis of $e^+e^- \to \gamma\gamma\pi^+\pi^-\ell^+\ell^-$ to constrain the sum of four momenta of the final state particles to that of the initial colliding beams. The χ^2 of the kinematic fit, $\chi^2_{\rm 4C}$, is required to be less than 40. If there are more than two photons in an event, the combination of $\gamma\gamma\pi^+\pi^-\ell^+\ell^-$ with the least $\chi^2_{\rm 4C}$ is retained for further study.

To identify signal candidates that involve the J/ψ resonance, we select events with a $\ell^+\ell^-$ invariant mass within a window of three detector resolutions from the J/ψ nominal mass [16], $3064.6 < M(\ell^+\ell^-) < 3140.8\,{\rm MeV}/c^2$, referred to as the J/ψ mass window. To remove the background from process $e^+e^- \to \eta' J/\psi$ with $\eta' \to \pi^+\pi^-\eta$, the invariant mass of $\pi^+\pi^-\gamma\gamma$ is required to be larger than 1 GeV/c^2. Two-dimensional (2D) distributions for $\gamma\gamma$ and $\pi^+\pi^- J/\psi$ invariant masses, $M(\gamma\gamma)$ versus $M(\pi^+\pi^- J/\psi)$, and the corresponding one-dimensional (1D) projections for data, signal MC samples, background contributions at $\sqrt{s} = 4.258\,{\rm GeV}$ are presented in figures 1(a-e). The distributions for the sum of 14 energy points are shown in figures 1(f-j). To select the signal candidates, the $\gamma\gamma$ combination is required to be within three detector resolutions from the known η mass [16], $507.1 < M(\gamma\gamma) < 579.1\,{\rm MeV}/c^2$, and the $\pi^+\pi^- J/\psi$ combination is required to be within three detector resolutions from the known $\psi(2S)$ mass [16], $3680.3 < M(\pi^+\pi^- J/\psi) <$

JHEP10(2021)177

Decay mode (Branching fraction)		
$e^+e^- \to \pi^+\pi^-\psi(2S)$,	$\psi(2S) \to J/\psi\eta$ (3.37%),	$\eta \to \gamma\gamma$ (39.41%)
$e^+e^- \to \pi^+\pi^-\psi(2S)$,	$\psi(2S) \to \gamma\chi_{c0}$ (9.79%),	$\chi_{c0} \to \gamma J/\psi$ (1.4%)
$e^+e^- \to \pi^+\pi^-\psi(2S)$,	$\psi(2S) \to \gamma\chi_{c1}$ (9.75%),	$\chi_{c1} \to \gamma J/\psi$ (34.3%)
$e^+e^- \to \pi^+\pi^-\psi(2S)$,	$\psi(2S) \to \gamma\chi_{c2}$ (9.52%),	$\chi_{c2} \to \gamma J/\psi$ (19.0%)
$e^+e^- \to \pi^0\pi^0\psi(2S)$,	$\psi(2S) \to \pi^+\pi^- J/\psi$ (34.68%)	
$e^+e^- \to \omega\chi_{c0}$,	$\omega \to \pi^+\pi^-\pi^0$ (89.3%),	$\chi_{c0} \to \gamma J/\psi$ (1.4%)
$e^+e^- \to \omega\chi_{c1}$,	$\omega \to \pi^+\pi^-\pi^0$ (89.3%),	$\chi_{c1} \to \gamma J/\psi$ (34.3%)
$e^+e^- \to \omega\chi_{c2}$,	$\omega \to \pi^+\pi^-\pi^0$ (89.3%),	$\chi_{c2} \to \gamma J/\psi$ (19.0%)
$e^+e^- \to \gamma X(3872)$,	$X(3872) \to \omega J/\psi$ (2.3%),	$\omega \to \pi^+\pi^-\pi^0$ (89.3%)
$e^+e^- \to \phi\chi_{c1}$,	$\phi \to \pi^+\pi^-\pi^0$ (15.24%),	$\chi_{c1} \to \gamma J/\psi$ (34.3%)
$e^+e^- \to \phi\chi_{c2}$,	$\phi \to \pi^+\pi^-\pi^0$ (15.24%),	$\chi_{c2} \to \gamma J/\psi$ (19.0%)
$e^+e^- \to \gamma\gamma\psi(2S)$,	$\psi(2S) \to \pi^+\pi^- J/\psi$ (34.68%)	

Table 1. The background processes (all J/ψ mesons decay into $\ell^+\ell^-$).

3692.5 MeV/c^2 (as indicated by red dashed boxes or the ranges between two arrows in figure 1). Significant clusters can be seen in the mass windows of the η and $\psi(2S)$.

4 Background analysis

To study background processes, we generated a series of MC samples for final states that include a $\pi^+\pi^-$ pair, two leptons with high momenta, and at least two photons in the final state using the KKMC generator at each energy point. These background processes are listed in table 1. The dominant background contribution is $e^+e^- \to \gamma\gamma\psi(2S)$, and it is measured directly in this analysis. The yields for each of the other background processes in the 2D signal region ($N_{\mathrm{bkg},i}$) are calculated using external input by:

$$N_{\mathrm{bkg},i} = \mathcal{L}_{\mathrm{int}}(1+\delta)_i|1-\Pi|^{-2}\epsilon_i\mathcal{B}_i\sigma^{\mathrm{B}}_{\mathrm{bkg},i}, \tag{4.1}$$

where i represents each background channel; $\mathcal{L}_{\mathrm{int}}$ is the integrated luminosity; $|1-\Pi|^{-2}$ is the vacuum polarization factor [44]; ϵ_i and $\mathcal{B}_i$ are the selection efficiency and the product branching fraction of the intermediate states taken from the PDG [16] for the ith background mode, respectively; and $\sigma^{\mathrm{B}}_{\mathrm{bkg},i}$ is the measured Born cross section of the ith background mode. The production cross sections for these background processes are taken from refs. [21, 45–50]. Assuming an input lineshape from refs. [21, 45–50], ISR correction factor $(1+\delta)_i$ is obtained from a quantum electrodynamics calculation [41, 42, 51] using the KKMC generator.

The irreducible background process $e^+e^- \to \gamma\gamma\psi(2S)$, $\psi(2S) \to \pi^+\pi^- J/\psi$, $J/\psi \to \ell^+\ell^-$ with the two photons not from resonance decay has the same final state particles as the signal channel; thus we measure its yield with the data directly. After applying all

JHEP10(2021)177

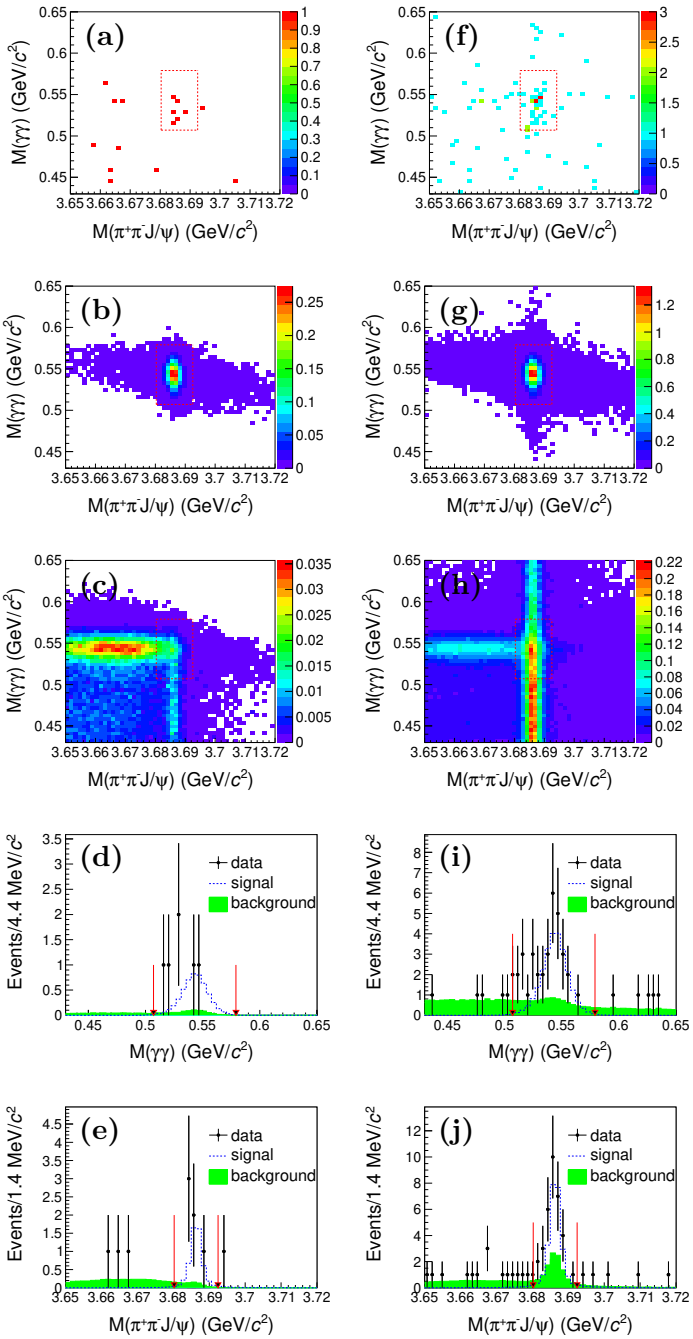

Figure 1. Two-dimensional distributions of $M(\gamma\gamma)$ versus $\mathrm{M}(\pi^+\pi^- J/\psi)$ for (a) data, (b) signal MC simulation, and (c) background MC contributions with the red dashed boxes for the defined η and $\psi(2S)$ signal regions, and the corresponding projections of (d) $M(\gamma\gamma)$ distribution in the $\psi(2S)$ mass window and (e) $M(\pi^+\pi^- J/\psi)$ distribution in the η mass window with red arrows for the defined signal regions at $\sqrt{s} = 4.258\,\mathrm{GeV}$, where the dots with error bars, the dashed blue lines, and the green histograms represent data, signal MC, and background MC simulations, respectively. The same distributions for the sum of the 14 data samples and MC samples are shown in (f), (g), (h), (i), and (j) correspondingly.

JHEP10(2021)177

$\sqrt{s}$ (GeV)	$N^0_{\gamma\gamma\psi(2S)}$	F
4.236	$5.94^{+3.12}_{-2.40}$	0.11
4.242	$1.79^{+1.80}_{-1.16}$	0.13
4.244	$5.99^{+2.80}_{-2.12}$	0.13
4.258	$1.35^{+2.49}_{-1.35}$	0.18
4.267	$1.81^{+2.13}_{-1.40}$	0.21
4.278	$2.48^{+2.53}_{-1.81}$	0.24
4.308	$0.00^{+1.29}_{-0.00}$	0.26
4.358	$5.04^{+3.12}_{-2.44}$	0.25
4.387	$0.00^{+1.29}_{-0.00}$	0.24
4.416	$11.28^{+4.49}_{-3.79}$	0.23
4.467	$2.25^{+2.12}_{-1.34}$	0.20
4.527	$0.00^{+1.29}_{-0.00}$	0.18
4.575	$1.00^{+1.36}_{-0.70}$	0.16
4.600	$4.02^{+2.97}_{-2.34}$	0.15

Table 2. The number of $e^+e^- \to \gamma\gamma\psi(2S)$ events outside the η signal region [$N^0_{\gamma\gamma\psi(2S)}$] and the F factor at each c.m. energy.

the selection criteria as for signal but the η mass window, we veto processes from $e^+e^- \to \gamma_{\rm ISR}\psi(2S)$, $e^+e^- \to \pi^0\psi(2S)$, and $e^+e^- \to \eta\psi(2S)$ by requiring the mass range of $\gamma\gamma$ larger than $300\,{\rm MeV}/c^2$ and not in $[507.1, 579.1]\,{\rm MeV}/c^2$. We fit $M(\pi^+\pi^- J/\psi)$ distribution of data using the line shape of MC simulated $e^+e^- \to \gamma\gamma\psi(2S)$ events to obtain the number of $e^+e^- \to \gamma\gamma\psi(2S)$ events [$N^0_{\gamma\gamma\psi(2S)}$] at each c.m. energy. The number of $e^+e^- \to \gamma\gamma\psi(2S)$ events in the η and $\psi(2S)$ signal regions [$N^1_{\gamma\gamma\psi(2S)}$] is obtained from the $N^0_{\gamma\gamma\psi(2S)}$ as follows:

$$N^1_{\gamma\gamma\psi(2S)} = F \cdot N^0_{\gamma\gamma\psi(2S)}, \tag{4.2}$$

$$F = \frac{\epsilon^1_e \mathcal{B}_e + \epsilon^1_\mu \mathcal{B}_\mu}{\epsilon^0_e \mathcal{B}_e + \epsilon^0_\mu \mathcal{B}_\mu}, \tag{4.3}$$

where F is a factor constructed from branching fractions and selection efficiencies; ϵ^1_e and ϵ^1_μ are the detection efficiencies for $J/\psi \to e^+e^-$ and $J/\psi \to \mu^+\mu^-$ decay channels in the η and $\psi(2S)$ signal regions, respectively; ϵ^0_e and ϵ^0_μ are the detection efficiencies for $J/\psi \to e^+e^-$ and $J/\psi \to \mu^+\mu^-$ decay channels, respectively, in the $\psi(2S)$ signal region but outside the η signal region; $\mathcal{B}_e$ and $\mathcal{B}_\mu$ are the branching fractions of decays $J/\psi \to e^+e^-$, and $J/\psi \to \mu^+\mu^-$, respectively [16]. The number of $e^+e^- \to \gamma\gamma\psi(2S)$ events in the $\psi(2S)$ signal region but outside the η signal region [$N^0_{\gamma\gamma\psi(2S)}$] and the F factor at each c.m. energy are listed in table 2.

The total number of background events ($n^{\rm b}$) in the 2D signal region is obtained with

$$n^{\rm b} = \sum_i N_{{\rm bkg},i} + N^1_{\gamma\gamma\psi(2S)}. \tag{4.4}$$

JHEP10(2021)177

Finally, the total numbers of background events in the signal region at different energy points, together with the numbers of background events from different final states are listed in table 3. The uncertainty on F is neglected, since it is too little to affect the number of $e^+e^- \to \gamma\gamma\psi(2S)$ events in the signal region. Therefore, the uncertainties on numbers of $e^+e^- \to \gamma\gamma\psi(2S)$ events are statistical only, and the uncertainties on numbers of other background events in table 3 are statistical and systematic.

5 Cross section measurement

It is assumed that the number of observed events ($n^{\rm obs}$) with the numbers of expected background ($n^{\rm b}$) and signal (μ) events in the signal region, follows a Poisson distribution,

$$P(n^{\rm obs};\mu,n^{\rm b}) = \frac{(\mu+n^{\rm b})^{n^{\rm obs}}}{n^{\rm obs}!}e^{-(\mu+n^{\rm b})}. \tag{5.1}$$

There are some energy points where the number of observed events is zero, but the number of background events is non-zero, such as $\sqrt{s} = 4.244\,\text{GeV}$ in table 4. Using the same method as in ref. [52], the value of μ with the maximum $P(n^{\rm obs};\mu,n^{\rm b})$ is taken as the non-negative number of signal events ($n^{\rm sig}$). Thus, $n^{\rm sig} = \max(0,\ n^{\rm obs} - n^{\rm b})$ is the best estimation of the number of signal events in the physically-allowed region.

The statistical uncertainty of the number of signal events at a 68.27% C.L. is estimated with the Feldman-Cousins (FC) method [52]. Since no significant $\eta\psi(2S)$ signal events are observed at some energy pints, the confidence intervals with the lower and upper limits at a 90% C.L. for the number of signal events are obtained with the Poissonian limit estimator (POLE) computer program [53].

The Born cross section of $e^+e^- \to \eta\psi(2S)$ is calculated with

$$\sigma^{\rm B} = \frac{n^{\rm sig}}{\mathcal{L}_{\rm int}(1+\delta)|1-\Pi|^{-2}\mathcal{B}_1\mathcal{B}_2(\epsilon_e\mathcal{B}_e+\epsilon_\mu\mathcal{B}_\mu)}, \tag{5.2}$$

where $\mathcal{B}_1$ and $\mathcal{B}_2$ are the branching fractions of $\psi(2S) \to \pi^+\pi^- J/\psi$ and $\eta \to \gamma\gamma$ [16], respectively; $(1+\delta)$ is the radiative correction factor obtained from the quantum electrodynamics calculation [41, 42, 51] using the KKMC generator, assuming an input lineshape of the $Y(4260)$ cross section [16]. The Born cross sections (and the confidence intervals with the lower and upper limits at the 90% C.L.), and the numbers used in the calculation are listed in table 4. Figure 2 shows the measured Born cross sections for $e^+e^- \to \eta\psi(2S)$ as a function of the collision energy. The statistical uncertainties of the cross sections at some energy points are different due to different accumulated luminosities.

The P-value is obtained by calculating the probability of the expected number of background events to fluctuate to the number of observed events or more in the signal region assuming a Poisson distribution. The total number of observed events is 34 in the sum of the 14 data samples at different c.m. energies. The total number of the background events in this analysis is 10.77 ± 1.85, where the uncertainty combines statistical and systematic ones. Considering the statistical and systematic uncertainties of background events, the P-value and the corresponding statistical significance of $e^+e^- \to \eta\psi(2S)$ signals from the

JHEP10(2021)177

$\sqrt{s}$ (GeV)	4.236	4.242	4.244	4.258	4.267	4.278	4.308
$\pi^+\pi^-\psi(2S),\psi(2S)\to J/\psi\eta$	<0.005	<0.005	0.01	0.49±0.05	0.87	0.39	0.03±0.01
$\pi^+\pi^-\psi(2S),\psi(2S)\to\gamma\chi_{c0}$	<0.005	<0.005	<0.005	0.01	0.02	0.01	<0.005
$\pi^+\pi^-\psi(2S),\psi(2S)\to\gamma\chi_{c1}$	<0.005	<0.005	<0.005	0.08±0.01	0.13	0.05	0.01
$\pi^+\pi^-\psi(2S),\psi(2S)\to\gamma\chi_{c2}$	<0.005	<0.005	<0.005	<0.005	<0.005	<0.005	<0.005
$\pi^0\pi^0\psi(2S)$	<0.005	<0.005	0.00±0.02	0.04±0.01	0.02	0.01	0.00±0.01
$\omega\chi_{c0}$	<0.005	<0.005	<0.005	<0.005	<0.005	<0.005	<0.005
$\omega\chi_{c1}$	—	—	—	—	—	—	0.00±0.01
$\omega\chi_{c2}$	—	—	—	—	—	—	—
$\gamma X(3872)$	—	—	—	—	—	—	—
$\phi\chi_{c1}$	—	—	—	—	—	—	—
$\phi\chi_{c2}$	—	—	—	—	—	—	—
$\gamma\gamma\psi(2S)$	$0.63^{+0.33}_{-0.25}$	$0.22^{+0.23}_{-0.15}$	$0.78^{+0.36}_{-0.27}$	$0.25^{+0.46}_{-0.25}$	$0.38^{+0.45}_{-0.29}$	$0.59^{+0.60}_{-0.43}$	$0.00^{+0.34}_{-0.00}$
$n^{\rm b}$	0.63±0.33	0.22±0.23	0.79±0.36	0.88±0.46	1.41±0.45	1.06±0.60	0.04±0.34
$\sqrt{s}$ (GeV)	4.358	4.387	4.416	4.467	4.527	4.575	4.600
$\pi^+\pi^-\psi(2S),\psi(2S)\to J/\psi\eta$	<0.005	<0.005	<0.005	—	—	—	—
$\pi^+\pi^-\psi(2S),\psi(2S)\to\gamma\chi_{c0}$	<0.005	<0.005	<0.005	—	—	—	—
$\pi^+\pi^-\psi(2S),\psi(2S)\to\gamma\chi_{c1}$	<0.005	<0.005	<0.005	—	—	—	—
$\pi^+\pi^-\psi(2S),\psi(2S)\to\gamma\chi_{c2}$	<0.005	<0.005	<0.005	—	—	—	—
$\pi^0\pi^0\psi(2S)$	0.20±0.03	0.00±0.03	0.29±0.04	0.00±0.02	0.00±0.02	0.00±0.01	0.02±0.01
$\omega\chi_{c0}$	<0.005	<0.005	<0.005	<0.005	<0.005	<0.005	<0.005
$\omega\chi_{c1}$	0.00±0.01	0.00±0.01	0.00±0.04	0.00±0.01	<0.005	—	—
$\omega\chi_{c2}$	0.00±0.05	0.00±0.02	0.16±0.03	0.00±0.02	<0.005	<0.005	0.00±0.01
$\gamma X(3872)$	<0.005	—	<0.005	—	—	—	<0.005
$\phi\chi_{c1}$	—	—	—	—	—	—	<0.005
$\phi\chi_{c2}$	—	—	—	—	—	—	<0.005
$\gamma\gamma\psi(2S)$	$1.28^{+0.79}_{-0.62}$	$0.00^{+0.31}_{-0.00}$	$2.57^{+1.02}_{-0.86}$	$0.44^{+0.42}_{-0.26}$	$0.00^{+0.23}_{-0.00}$	$0.16^{+0.22}_{-0.11}$	$0.59^{+0.44}_{-0.34}$
$n^{\rm b}$	1.49±0.80	0.00±0.31	3.03±1.02	0.44±0.42	0.00±0.23	0.16±0.22	0.62±0.44

Table 3. The total numbers of background events in the signal region ($n^{\rm b}$) at different energy points, together with the numbers of background events from different final states. Ellipses mean that the results are not applicable. The numbers of background events which are less than 0.005, are represented with < 0.005. The asymmetric uncertainty for the number of $e^+e^-\to\gamma\gamma\psi(2S)$ events [$N^1_{\gamma\gamma\psi(2S)}$] is obtained with the eq. (4.2), which is associated with the asymmetric uncertainty of $N^0_{\gamma\gamma\psi(2S)}$ and F. The symmetric uncertainties for the numbers of other individual background sources are calculated with eq. (4.1), and are dominated by the uncertainties of the input cross sections [21, 45–50]. For the numbers of background events with uncertainties less than 0.005, only the mean values are quoted in the table. The ratio of the uncertainty in the number of background events to the number of signal events is taken as the systematic uncertainty on the background estimation.

JHEP10(2021)177

$\sqrt{s}$ (GeV)	$\mathcal{L}_{\rm int}$ (pb^{-1})	$n^{\rm obs}$	$n^{\rm b}$	$n^{\rm sig}$	$n^{\rm sig}_{\rm POLE}$	$\Sigma(10^{-2})$	$(1+\delta)$	$\lvert 1-\Pi\rvert^{-2}$	σ^B (pb)	$\sigma^{\rm B}_{\rm POLE}$ (pb)
4.236	530.3	2	0.63 ± 0.33	$1.4^{+2.2}_{-1.0}$	(0.0, 5.9)	0.430	0.76	1.056	$0.8^{+1.2}_{-0.5}$	(0.0, 3.2)
4.242	55.9	0	0.22 ± 0.23	$0.0^{+1.1}_{-0.0}$	(0.0, 2.5)	0.430	0.76	1.055	$0.0^{+5.7}_{-0.0}$	(0.0, 12.9)
4.244	538.1	0	0.79 ± 0.36	$0.0^{+0.7}_{-0.0}$	(0.0, 2.5)	0.422	0.77	1.056	$0.0^{+0.4}_{-0.0}$	(0.0, 1.4)
4.258	828.4	6	0.88 ± 0.46	$5.1^{+3.3}_{-2.1}$	(1.6, 10.9)	0.412	0.78	1.054	$1.8^{+1.2}_{-0.8}$	(0.6, 3.9)
4.267	531.1	7	1.41 ± 0.45	$5.6^{+3.3}_{-2.8}$	(2.1, 11.8)	0.399	0.79	1.053	$3.2^{+1.9}_{-1.6}$	(1.2, 6.7)
4.278	175.7	2	1.06 ± 0.60	$0.9^{+2.3}_{-0.8}$	(0.0, 8.0)	0.384	0.82	1.053	$1.5^{+3.9}_{-1.4}$	(0.0, 13.7)
4.308	45.1	0	0.04 ± 0.34	$0.0^{+1.3}_{-0.0}$	(0.0, 2.4)	0.351	0.94	1.052	$0.0^{+8.3}_{-0.0}$	(0.0, 15.3)
4.358	543.9	3	1.49 ± 0.80	$1.5^{+2.3}_{-1.2}$	(0.0, 9.2)	0.281	1.18	1.051	$0.8^{+1.2}_{-0.6}$	(0.0, 4.9)
4.387	55.6	0	0.00 ± 0.31	$0.0^{+1.3}_{-0.0}$	(0.0, 2.5)	0.252	1.32	1.051	$0.0^{+6.7}_{-0.0}$	(0.0, 12.9)
4.416	1043.9	8	3.03 ± 1.02	$5.0^{+3.3}_{-2.7}$	(1.4, 12.4)	0.223	1.46	1.052	$1.4^{+0.9}_{-0.8}$	(0.4, 3.5)
4.467	111.1	4	0.44 ± 0.42	$3.6^{+2.7}_{-1.7}$	(1.2, 8.4)	0.194	1.72	1.055	$9.2^{+6.9}_{-4.4}$	(3.1, 21.5)
4.527	112.1	0	0.00 ± 0.23	$0.0^{+1.3}_{-0.0}$	(0.0, 2.4)	0.166	2.02	1.054	$0.0^{+3.3}_{-0.0}$	(0.0, 6.1)
4.575	48.9	0	0.16 ± 0.22	$0.0^{+1.1}_{-0.0}$	(0.0, 2.4)	0.151	2.25	1.054	$0.0^{+6.2}_{-0.0}$	(0.0, 13.6)
4.600	586.9	2	0.62 ± 0.44	$1.4^{+2.2}_{-1.0}$	(0.0, 6.2)	0.143	2.38	1.055	$0.7^{+1.0}_{-0.5}$	(0.0, 2.9)
Sum		34	10.77 ± 1.85		P-value	4.6×10^{-7}		Statistical significance		4.9σ

Table 4. The cross sections $\sigma^{\rm B}$ and the confidence intervals with the lower and upper limits on $\sigma^{\rm B}$ with the POLE ($\sigma^{\rm B}_{\rm POLE}$) method for $e^+e^- \to \eta\psi(2S)$ at different energy points, together with integrated luminosities $\mathcal{L}_{\rm int}$, numbers of observed events $n^{\rm obs}$, background events $n^{\rm b}$, and signal events $n^{\rm sig}$, the confidence intervals with the lower and upper limits for the numbers of signal events $n^{\rm sig}_{\rm POLE}$, products of detection efficiencies and branching fractions $\Sigma = \mathcal{B}_1\mathcal{B}_2(\epsilon_e\mathcal{B}_e + \epsilon_\mu\mathcal{B}_\mu)$, ISR correction factors $(1+\delta)$, vacuum polarization factors $\lvert 1-\Pi\rvert^{-2}$, the P-value, and the statistical significance. The uncertainties of $n^{\rm sig}$ and $\sigma^{\rm B}$ are statistical only. All limits are given at 90% confidence level.

JHEP10(2021)177

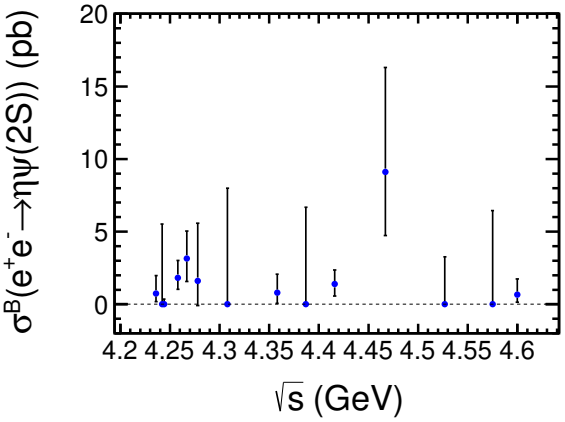

Figure 2. The measured Born cross section as a function of the collision energy. The uncertainties are statistical only.

5.25 fb^{-1} BESIII data are 4.6×10^{-7} and 4.9 standard deviations (σ), respectively, which are listed in table 4.

6 Systematic uncertainties

The systematic uncertainties in the cross-section measurement mainly come from the luminosity, tracking efficiency, photon detection efficiency, the branching fractions of intermediate particle decays, ISR correction factor, kinematic fit, background estimation, and mass windows of J/ψ, η, and $\psi(2S)$ mesons. The uncertainty from the vacuum polarization is negligible. Different systematic uncertainties at the same energy are assumed to be uncorrelated, and that systematic uncertainties between different energies are assumed to be fully correlated.

- *Luminosity.* The integrated luminosity was measured using Bhabha scattering events with an uncertainty of 1.0% [34, 35], which is taken as the systematic uncertainty.

- *Tracking efficiency.* The uncertainty of the tracking efficiency is 1.0% per track, which is taken from ref. [29].

- *Photon detection efficiency.* The uncertainty from photon reconstruction is 1.0% per photon, which is determined from the study of the process $J/\psi \to \rho^0\pi^0$, $\rho^0 \to \pi^+\pi^-$, $\pi^0 \to \gamma\gamma$ [54].

- *Branching fraction.* The uncertainties on the branching fractions of the intermediate states are taken from the PDG [16].

- *ISR correction factor.* Due to insufficient information from previous experiments, we obtain the ISR correction factor according to the decay of the $Y(4260)$ resonant structure in this work. Changing the Breit-Wigner (BW) function for the $Y(4260)$

JHEP10(2021)177

to that for the $\psi(4415)$, the difference between these two assumptions is taken as the systematic uncertainty.

- *Kinematic fit.* The systematic uncertainty from the kinematic fit is estimated by correcting the helix parameters of charged tracks according to the method described in ref. [55]. The MC sample with the track helix parameter correction applied is taken as the nominal one. The difference between detection efficiencies obtained from MC samples with and without correction is taken as the uncertainty.

- *Background estimation.* From eq. (4.1), the number of background events is estimated using the measured cross sections. The ratio of the uncertainty in the number of background events to the number of signal events is taken as the uncertainty of the background estimation.

- *Mass window.* The mass resolution discrepancy between MC simulation and the data will lead to a bias in the efficiency determination when a mass window requirement is applied to the invariant mass distribution. The process $e^+e^- \to \pi^+\pi^-\psi(2S)$ with $\psi(2S) \to \eta J/\psi$ at $\sqrt{s} = 4.416\,\text{GeV}$ is taken as the control sample to estimate the uncertainty due to the J/ψ and η mass windows. The discrepancies in efficiency between data and MC samples for J/ψ and η mass windows are $(0.80 \pm 0.12)\%$ and $(-0.35 \pm 2.27)\%$, respectively. The uncertainties of J/ψ and η mass windows are quoted as 0.92% and 2.62%, respectively. The uncertainty of the $\psi(2S)$ mass window is determined to be 2.3%, using a large data sample observed in $e^+e^- \to \pi^+\pi^-\psi(2S)$ [45]. Finally, the total systematic uncertainty on mass windows is 3.6% by adding these numbers in quadrature.

Table 5 summarizes the systematic uncertainties from all the sources. The total systematic uncertainty is obtained by summing the individual uncertainties in quadrature, assuming that all sources are independent.

7 Summary

In summary, using 5.25 fb^{-1} data collected at c.m. energies from 4.236 to 4.600 GeV, the process $e^+e^- \to \eta\psi(2S)$ is observed for the first time with a 4.9σ statistical significance. The energy-dependent cross section has been measured and the results are listed in table 4. Because of the limited statistics, the signals at some energy points are not significant, thus it is impossible to extract the couplings of the Y states to $\eta\psi(2S)$ from a fit to the cross sections of $e^+e^- \to \eta\psi(2S)$. Further experimental studies with higher statistics are needed to draw a clear conclusion on the structure in the $e^+e^- \to \eta\psi(2S)$ process. BESIII plans to collect additional data samples over a variety of c.m. energies in the future [56]. Furthermore, a partial event reconstruction technique with a missing track may improve the detection efficiency of this process. This will allow us to study the structure of the $\eta\psi(2S)$ and explore the nature of the vector charmonium-like states.

JHEP10(2021)177

$\sqrt{s}$ (GeV)	Luminosity	Tracking	Photon	BR	ISR	Kinematic fit	Background	Mass window	Sum
4.236	1.0	4.0	2.0	1.2	10.4	2.6	23.6	3.6	26.6
4.242	1.0	4.0	2.0	1.2	10.9	2.6	—	3.6	12.7
4.244	1.0	4.0	2.0	1.2	10.5	2.8	—	3.6	12.4
4.258	1.0	4.0	2.0	1.2	7.4	2.7	9.0	3.6	13.4
4.267	1.0	4.0	2.0	1.2	5.3	3.1	8.0	3.6	11.7
4.278	1.0	4.0	2.0	1.2	2.4	3.1	66.7	3.6	67.0
4.308	1.0	4.0	2.0	1.2	5.1	3.2	—	3.6	8.5
4.358	1.0	4.0	2.0	1.2	10.6	3.5	53.3	3.6	54.8
4.387	1.0	4.0	2.0	1.2	12.4	3.5	—	3.6	14.2
4.416	1.0	4.0	2.0	1.2	11.4	3.1	20.4	3.6	24.3
4.467	1.0	4.0	2.0	1.2	2.0	3.3	11.7	3.6	13.6
4.527	1.0	4.0	2.0	1.2	1.2	3.1	—	3.6	6.8
4.575	1.0	4.0	2.0	1.2	4.4	2.8	—	3.6	7.9
4.600	1.0	4.0	2.0	1.2	5.0	2.9	31.4	3.6	32.5

Table 5. The relative systematic uncertainties from luminosity, tracking efficiency, photon detection efficiency, branching fraction (BR), ISR correction factor, kinematic fit, background estimation, and mass windows (in units of %). Ellipses mean that the results are not applicable.

Acknowledgments

The BESIII collaboration thanks the staff of BEPCII and the IHEP computing center for their strong support. This work is supported in part by National Key Research and Development Program of China under Contracts Nos. 2020YFA0406300, 2020YFA0406400; National Natural Science Foundation of China (NSFC) under Contracts Nos. 11625523, 11635010, 11735014, 11822506, 11835012, 11935015, 11935016, 11935018, 11961141012; the Chinese Academy of Sciences (CAS) Large-Scale Scientific Facility Program; Joint Large-Scale Scientific Facility Funds of the NSFC and CAS under Contracts Nos. U1732263, U1832207; CAS Key Research Program of Frontier Sciences under Contracts Nos. QYZDJ-SSW-SLH003, QYZDJ-SSW-SLH040; 100 Talents Program of CAS; INPAC and Shanghai Key Laboratory for Particle Physics and Cosmology; ERC under Contract No. 758462; European Union Horizon 2020 research and innovation programme under Contract No. Marie Sklodowska-Curie grant agreement No 894790; German Research Foundation DFG under Contracts Nos. 443159800, Collaborative Research Center CRC 1044, FOR 2359, FOR 2359, GRK 214; Istituto Nazionale di Fisica Nucleare, Italy; Ministry of Development of Turkey under Contract No. DPT2006K-120470; National Science and Technology fund; Olle Engkvist Foundation under Contract No. 200-0605; STFC (United Kingdom); The Knut and Alice Wallenberg Foundation (Sweden) under Contract No. 2016.0157; The Royal Society, U.K. under Contracts Nos. DH140054, DH160214; The Swedish Research Council; U.S. Department of Energy under Contracts Nos. DE-FG02-05ER41374, DE-SC-0012069.

References

[1] H.-X. Chen, W. Chen, X. Liu and S.-L. Zhu, *The hidden-charm pentaquark and tetraquark states*, *Phys. Rept.* **639** (2016) 1 [arXiv:1601.02092] [INSPIRE].

[2] A. Esposito, A. Pilloni and A.D. Polosa, *Multiquark resonances*, *Phys. Rept.* **668** (2017) 1 [arXiv:1611.07920] [INSPIRE].

[3] R.F. Lebed, R.E. Mitchell and E.S. Swanson, *Heavy-quark QCD exotica*, *Prog. Part. Nucl. Phys.* **93** (2017) 143 [arXiv:1610.04528] [INSPIRE].

[4] A. Ali, J.S. Lange and S. Stone, *Exotics: heavy pentaquarks and tetraquarks*, *Prog. Part. Nucl. Phys.* **97** (2017) 123 [arXiv:1706.00610] [INSPIRE].

[5] S.L. Olsen, T. Skwarnicki and D. Zieminska, *Nonstandard heavy mesons and baryons: experimental evidence*, *Rev. Mod. Phys.* **90** (2018) 015003 [arXiv:1708.04012] [INSPIRE].

[6] F.-K. Guo, C. Hanhart, U.-G. Meißner, Q. Wang, Q. Zhao and B.-S. Zou, *Hadronic molecules*, *Rev. Mod. Phys.* **90** (2018) 015004 [arXiv:1705.00141] [INSPIRE].

[7] N. Brambilla et al., *The XYZ states: experimental and theoretical status and perspectives*, *Phys. Rept.* **873** (2020) 1 [arXiv:1907.07583] [INSPIRE].

[8] BaBar collaboration, *Observation of a broad structure in the $\pi^+\pi^- J/\psi$ mass spectrum around 4.26 GeV/c^2*, *Phys. Rev. Lett.* **95** (2005) 142001 [hep-ex/0506081] [INSPIRE].

JHEP10(2021)177

[9] CLEO collaboration, *Confirmation of the $Y(4260)$ resonance production in initial state radiation*, *Phys. Rev. D* **74** (2006) 091104 [hep-ex/0611021] [INSPIRE].

[10] BELLE collaboration, *Measurement of $e^+e^- \to \pi^+\pi^- J/\psi$ cross-section via initial state radiation at Belle*, *Phys. Rev. Lett.* **99** (2007) 182004 [arXiv:0707.2541] [INSPIRE].

[11] BABAR collaboration, *Study of the reaction $e^+e^- \to J/\psi\pi^+\pi^-$ via initial-state radiation at BaBar*, *Phys. Rev. D* **86** (2012) 051102 [arXiv:1204.2158] [INSPIRE].

[12] BELLE collaboration, *Study of $e^+e^- \to \pi^+\pi^- J/\psi$ and observation of a charged charmoniumlike state at Belle*, *Phys. Rev. Lett.* **110** (2013) 252002 [*Erratum ibid.* **111** (2013) 019901] [arXiv:1304.0121] [INSPIRE].

[13] BABAR collaboration, *Evidence of a broad structure at an invariant mass of 4.32 GeV/c^2 in the reaction $e^+e^- \to \pi^+\pi^-\psi(2S)$ measured at BaBar*, *Phys. Rev. Lett.* **98** (2007) 212001 [hep-ex/0610057] [INSPIRE].

[14] BELLE collaboration, *Observation of two resonant structures in $e^+e^- \to \pi^+\pi^-\psi(2S)$ via initial state radiation at Belle*, *Phys. Rev. Lett.* **99** (2007) 142002 [arXiv:0707.3699] [INSPIRE].

[15] BABAR collaboration, *Study of the reaction $e^+e^- \to \psi(2S)\pi^-\pi^-$ via initial-state radiation at BaBar*, *Phys. Rev. D* **89** (2014) 111103 [arXiv:1211.6271] [INSPIRE].

[16] PARTICLE DATA GROUP collaboration, *Review of particle physics*, *PTEP* **2020** (2020) 083C01 [INSPIRE].

[17] T. Barnes, S. Godfrey and E.S. Swanson, *Higher charmonia*, *Phys. Rev. D* **72** (2005) 054026 [hep-ph/0505002] [INSPIRE].

[18] BESIII collaboration, *Precise measurement of the $e^+e^- \to \pi^+\pi^- J/\psi$ cross section at center-of-mass energies from 3.77 to 4.60 GeV*, *Phys. Rev. Lett.* **118** (2017) 092001 [arXiv:1611.01317] [INSPIRE].

[19] BELLE collaboration, *Measurement of $e^+e^- \to \pi^+\pi^-\psi(2S)$ via initial state radiation at Belle*, *Phys. Rev. D* **91** (2015) 112007 [arXiv:1410.7641] [INSPIRE].

[20] BESIII collaboration, *Evidence of two resonant structures in $e^+e^- \to \pi^+\pi^- h_c$*, *Phys. Rev. Lett.* **118** (2017) 092002 [arXiv:1610.07044] [INSPIRE].

[21] BESIII collaboration, *Cross section measurements of $e^+e^- \to \omega\chi_{c0}$ from $\sqrt{s} = 4.178$ to 4.278 GeV*, *Phys. Rev. D* **99** (2019) 091103 [arXiv:1903.02359] [INSPIRE].

[22] BESIII collaboration, *Evidence of a resonant structure in the $e^+e^- \to \pi^+ D^0 D^{*-}$ cross section between 4.05 and 4.60 GeV*, *Phys. Rev. Lett.* **122** (2019) 102002 [arXiv:1808.02847] [INSPIRE].

[23] CLEO collaboration, *Charmonium decays of $Y(4260)$, $\psi(4160)$ and $\psi(4040)$*, *Phys. Rev. Lett.* **96** (2006) 162003 [hep-ex/0602034] [INSPIRE].

[24] BELLE collaboration, *Observation of $\psi(4040)$ and $\psi(4160)$ decay into $\eta J/\psi$*, *Phys. Rev. D* **87** (2013) 051101 [arXiv:1210.7550] [INSPIRE].

[25] BESIII collaboration, *Observation of $e^+e^- \to \eta J/\psi$ at center-of-mass energy $\sqrt{s} = 4.009$ GeV*, *Phys. Rev. D* **86** (2012) 071101 [arXiv:1208.1857] [INSPIRE].

[26] BESIII collaboration, *Measurement of the $e^+e^- \to \eta J/\psi$ cross section and search for $e^+e^- \to \pi^0 J/\psi$ at center-of-mass energies between 3.810 and 4.600 GeV*, *Phys. Rev. D* **91** (2015) 112005 [arXiv:1503.06644] [INSPIRE].

JHEP10(2021)177

[27] BESIII collaboration, *Observation of the $Y(4220)$ and $Y(4390)$ in the process $e^+e^- \to \eta J/\psi$*, *Phys. Rev. D* **102** (2020) 031101 [arXiv:2003.03705] [INSPIRE].

[28] C.-F. Qiao and R.-L. Zhu, *Understanding the cross section of $e^+e^- \to \eta J/\psi$ process via nonrelativistic QCD*, *Phys. Rev. D* **89** (2014) 074006 [arXiv:1403.1918] [INSPIRE].

[29] BESIII collaboration, *Observation of $e^+e^- \to \eta' J/\psi$ at center-of-mass energies between* 4.189 *and* 4.600 *GeV*, *Phys. Rev. D* **94** (2016) 032009 [arXiv:1605.03256] [INSPIRE].

[30] BESIII collaboration, *Cross section measurement of $e^+e^- \to \eta' J/\psi$ from $\sqrt{s} = 4.178$ to* 4.600 *GeV*, *Phys. Rev. D* **101** (2020) 012008 [arXiv:1911.00885] [INSPIRE].

[31] BESIII collaboration, *Design and construction of the BESIII detector*, *Nucl. Instrum. Meth. A* **614** (2010) 345 [arXiv:0911.4960] [INSPIRE].

[32] C.H. Yu et al., *BEPCII performance and beam dynamics studies on luminosity*, in *Proceedings of IPAC*2016, TUYA01, Busan, Korea, (2016).

[33] BESIII collaboration, *Measurements of the center-of-mass energies at BESIII via the di-muon process*, *Chin. Phys. C* **40** (2016) 063001 [arXiv:1510.08654] [INSPIRE].

[34] BESIII collaboration, *Precision measurement of the integrated luminosity of the data taken by BESIII at center of mass energies between* 3.810 *GeV and* 4.600 *GeV*, *Chin. Phys. C* **39** (2015) 093001 [arXiv:1503.03408] [INSPIRE].

[35] BESIII collaboration, *Luminosity measurements for the R scan experiment at BESIII*, *Chin. Phys. C* **41** (2017) 063001 [arXiv:1702.04977] [INSPIRE].

[36] X. Li et al., *Study of MRPC technology for BESIII endcap-TOF upgrade*, *Radiat. Detect. Technol. Methods* **1** (2017) 13.

[37] Y.X. Guo et al., *The study of time calibration for upgraded end cap TOF of BESIII*, *Radiat. Detect. Technol. Methods* **1** (2017) 15.

[38] GEANT4 collaboration, *GEANT4 — a simulation toolkit*, *Nucl. Instrum. Meth. A* **506** (2003) 250 [INSPIRE].

[39] D.J. Lange, *The EvtGen particle decay simulation package*, *Nucl. Instrum. Meth. A* **462** (2001) 152 [INSPIRE].

[40] R.-G. Ping, *Event generators at BESIII*, *Chin. Phys. C* **32** (2008) 599 [INSPIRE].

[41] S. Jadach, B.F.L. Ward and Z. Was, *The precision Monte Carlo event generator KK for two fermion final states in e^+e^- collisions*, *Comput. Phys. Commun.* **130** (2000) 260 [hep-ph/9912214] [INSPIRE].

[42] S. Jadach, B.F.L. Ward and Z. Was, *Coherent exclusive exponentiation for precision Monte Carlo calculations*, *Phys. Rev. D* **63** (2001) 113009 [hep-ph/0006359] [INSPIRE].

[43] E. Richter-Was, *QED bremsstrahlung in semileptonic B and leptonic τ decays*, *Phys. Lett. B* **303** (1993) 163 [INSPIRE].

[44] Working Group on Radiative Corrections and Monte Carlo Generators for Low Energies collaboration, *Quest for precision in hadronic cross sections at low energy: Monte Carlo tools vs. experimental data*, *Eur. Phys. J. C* **66** (2010) 585 [arXiv:0912.0749] [INSPIRE].

[45] BESIII collaboration, *Measurement of $e^+e^- \to \pi^+\pi^-\psi(3686)$ from* 4.008 *to* 4.600 *GeV and observation of a charged structure in the $\pi^\pm\psi(3686)$ mass spectrum*, *Phys. Rev. D* **96** (2017) 032004 [*Erratum ibid.* **99** (2019) 019903] [arXiv:1703.08787] [INSPIRE].

JHEP10(2021)177

[46] BESIII collaboration, *Measurement of $e^+e^- \to \pi^0\pi^0\psi(3686)$ at $\sqrt{s}$ from 4.009 to 4.600 GeV and observation of a neutral charmoniumlike structure*, *Phys. Rev. D* **97** (2018) 052001 [arXiv:1710.10740] [INSPIRE].

[47] BESIII collaboration, *Study of $e^+e^- \to \omega\chi_{cJ}$ at center-of-mass energies from 4.21 to 4.42 GeV*, *Phys. Rev. Lett.* **114** (2015) 092003 [arXiv:1410.6538] [INSPIRE].

[48] BESIII collaboration, *Observation of $e^+e^- \to \omega\chi_{c1,2}$ near $\sqrt{s} = 4.42$ and 4.6 GeV*, *Phys. Rev. D* **93** (2016) 011102 [arXiv:1511.08564] [INSPIRE].

[49] BESIII collaboration, *Study of $e^+e^- \to \gamma\omega J/\psi$ and observation of $X(3872) \to \omega J/\psi$*, *Phys. Rev. Lett.* **122** (2019) 232002 [arXiv:1903.04695] [INSPIRE].

[50] BESIII collaboration, *Observation of $e^+e^- \to \phi\chi_{c1}$ and $\phi\chi_{c2}$ at $\sqrt{s} = 4.600$ GeV*, *Phys. Rev. D* **97** (2018) 032008 [arXiv:1712.09240] [INSPIRE].

[51] E.A. Kuraev and V.S. Fadin, *On radiative corrections to e^+e^- single photon annihilation at high-energy*, *Sov. J. Nucl. Phys.* **41** (1985) 466 [*Yad. Fiz.* **41** (1985) 733] [INSPIRE].

[52] G.J. Feldman and R.D. Cousins, *Unified approach to the classical statistical analysis of small signals*, *Phys. Rev. D* **57** (1998) 3873 [physics/9711021] [INSPIRE].

[53] J. Conrad, *A program for confidence interval calculations for a Poisson process with background including systematic uncertainties: POLE* 1.0, *Comput. Phys. Commun.* **158** (2004) 117 [INSPIRE].

[54] BESIII collaboration, *Branching fraction measurements of χ_{c0} and χ_{c2} to $\pi^0\pi^0$ and $\eta\eta$*, *Phys. Rev. D* **81** (2010) 052005 [arXiv:1001.5360] [INSPIRE].

[55] BESIII collaboration, *Search for hadronic transition $\chi_{cJ} \to \eta_c\pi^+\pi^-$ and observation of $\chi_{cJ} \to K\bar{K}\pi\pi\pi$*, *Phys. Rev. D* **87** (2013) 012002 [arXiv:1208.4805] [INSPIRE].

[56] BESIII collaboration, *Future physics programme of BESIII*, *Chin. Phys. C* **44** (2020) 040001 [arXiv:1912.05983] [INSPIRE].

JHEP10(2021)177

The BESIII collaboration

M. Ablikim,[1] M.N. Achasov,[10,c] P. Adlarson,[67] S. Ahmed,[15] M. Albrecht,[4] R. Aliberti,[28] A. Amoroso,[66A,66C] M.R. An,[32] Q. An,[63,49] X.H. Bai,[57] Y. Bai,[48] O. Bakina,[29] R. Baldini Ferroli,[23A] I. Balossino,[24A] Y. Ban,[38,j] K. Begzsuren,[26] N. Berger,[28] M. Bertani,[23A] D. Bettoni,[24A] F. Bianchi,[66A,66C] J. Bloms,[60] A. Bortone,[66A,66C] I. Boyko,[29] R.A. Briere,[5] H. Cai,[68] X. Cai,[1,49] A. Calcaterra,[23A] G.F. Cao,[1,54] N. Cao,[1,54] S.A. Cetin,[53A] J.F. Chang,[1,49] W.L. Chang,[1,54] G. Chelkov,[29,b] D.Y. Chen,[6] G. Chen,[1] H.S. Chen,[1,54] M.L. Chen,[1,49] S.J. Chen,[35] X.R. Chen,[25] Y.B. Chen,[1,49] Z.J. Chen,[20,k] W.S. Cheng,[66C] G. Cibinetto,[24A] F. Cossio,[66C] X.F. Cui,[36] H.L. Dai,[1,49] X.C. Dai,[1,54] A. Dbeyssi,[15] R. E. de Boer,[4] D. Dedovich,[29] Z.Y. Deng,[1] A. Denig,[28] I. Denysenko,[29] M. Destefanis,[66A,66C] F. De Mori,[66A,66C] Y. Ding,[33] C. Dong,[36] J. Dong,[1,49] L.Y. Dong,[1,54] M.Y. Dong,[1,49,54] X. Dong,[68] S.X. Du,[71] Y.L. Fan,[68] J. Fang,[1,49] S.S. Fang,[1,54] Y. Fang,[1] R. Farinelli,[24A] L. Fava,[66B,66C] F. Feldbauer,[4] G. Felici,[23A] C.Q. Feng,[63,49] J.H. Feng,[50] M. Fritsch,[4] C.D. Fu,[1] Y. Gao,[64] Y. Gao,[38,j] Y. Gao,[63,49] Y.G. Gao,[6] I. Garzia,[24A,24B] P.T. Ge,[68] C. Geng,[50] E.M. Gersabeck,[58] A. Gilman,[61] K. Goetzen,[11] L. Gong,[33] W.X. Gong,[1,49] W. Gradl,[28] M. Greco,[66A,66C] L.M. Gu,[35] M.H. Gu,[1,49] S. Gu,[2] Y.T. Gu,[13] C.Y. Guan,[1,54] A.Q. Guo,[22] L.B. Guo,[34] R.P. Guo,[40] Y.P. Guo,[9,h] A. Guskov,[29,b] T.T. Han,[41] W.Y. Han,[32] X.Q. Hao,[16] F.A. Harris,[56] K.L. He,[1,54] F.H. Heinsius,[4] C.H. Heinz,[28] T. Held,[4] Y.K. Heng,[1,49,54] C. Herold,[51] M. Himmelreich,[11,f] T. Holtmann,[4] G.Y. Hou,[1,54] Y.R. Hou,[54] Z.L. Hou,[1] H.M. Hu,[1,54] J.F. Hu,[47,l] T. Hu,[1,49,54] Y. Hu,[1] G.S. Huang,[63,49] L.Q. Huang,[64] X.T. Huang,[41] Y.P. Huang,[1] Z. Huang,[38,j] T. Hussain,[65] N. Hüsken,[22,28] W. Ikegami Andersson,[67] W. Imoehl,[22] M. Irshad,[63,49] S. Jaeger,[4] S. Janchiv,[26] Q. Ji,[1] Q.P. Ji,[16] X.B. Ji,[1,54] X.L. Ji,[1,49] Y.Y. Ji,[41] H.B. Jiang,[41] X.S. Jiang,[1,49,54] J.B. Jiao,[41] Z. Jiao,[18] S. Jin,[35] Y. Jin,[57] M.Q. Jing,[1,54] T. Johansson,[67] N. Kalantar-Nayestanaki,[55] X.S. Kang,[33] R. Kappert,[55] M. Kavatsyuk,[55] B.C. Ke,[43,1] I.K. Keshk,[4] A. Khoukaz,[60] P. Kiese,[28] R. Kiuchi,[1] R. Kliemt,[11] L. Koch,[30] O.B. Kolcu,[53A,e] B. Kopf,[4] M. Kuemmel,[4] M. Kuessner,[4] A. Kupsc,[67] M. G. Kurth,[1,54] W. Kühn,[30] J.J. Lane,[58] J.S. Lange,[30] P. Larin,[15] A. Lavania,[21] L. Lavezzi,[66A,66C] Z.H. Lei,[63,49] H. Leithoff,[28] M. Lellmann,[28] T. Lenz,[28] C. Li,[39] C.H. Li,[32] Cheng Li,[63,49] D.M. Li,[71] F. Li,[1,49] G. Li,[1] H. Li,[63,49] H. Li,[43] H.B. Li,[1,54] H.J. Li,[16] J.L. Li,[41] J.Q. Li,[4] J.S. Li,[50] Ke Li,[1] L.K. Li,[1] Lei Li,[3] P.R. Li,[31,m,n] S.Y. Li,[52] W.D. Li,[1,54] W.G. Li,[1] X.H. Li,[63,49] X.L. Li,[41] Xiaoyu Li,[1,54] Z.Y. Li,[50] H. Liang,[1,54] H. Liang,[63,49] H. Liang,[27] Y.F. Liang,[45] Y.T. Liang,[25] G.R. Liao,[12] L.Z. Liao,[1,54] J. Libby,[21] C.X. Lin,[50] B.J. Liu,[1] C.X. Liu,[1] D. Liu,[15,63] F.H. Liu,[44] Fang Liu,[1] Feng Liu,[6] H.B. Liu,[13] H.M. Liu,[1,54] Huanhuan Liu,[1] Huihui Liu,[17] J.B. Liu,[63,49] J.L. Liu,[64] J.Y. Liu,[1,54] K. Liu,[1] K.Y. Liu,[33] L. Liu,[63,49] M.H. Liu,[9,h] P.L. Liu,[1] Q. Liu,[68] Q. Liu,[54] S.B. Liu,[63,49] Shuai Liu,[46] T. Liu,[1,54] W.M. Liu,[63,49] X. Liu,[31,m,n] Y. Liu,[31,m,n] Y.B. Liu,[36] Z.A. Liu,[1,49,54] Z.Q. Liu,[41] X.C. Lou,[1,49,54] F.X. Lu,[50] H.J. Lu,[18] J.D. Lu,[1,54] J.G. Lu,[1,49] X.L. Lu,[1] Y. Lu,[1] Y.P. Lu,[1,49] C.L. Luo,[34] M.X. Luo,[70] P.W. Luo,[50] T. Luo,[9,h] X.L. Luo,[1,49] X.R. Lyu,[54] F.C. Ma,[33] H.L. Ma,[1] L.L. Ma,[41] M.M. Ma,[1,54] Q.M. Ma,[1] R.Q. Ma,[1,54] R.T. Ma,[54] X.X. Ma,[1,54] X.Y. Ma,[1,49] F.E. Maas,[15] M. Maggiora,[66A,66C] S. Maldaner,[4] S. Malde,[61] A. Mangoni,[23B] Y.J. Mao,[38,j] Z.P. Mao,[1] S. Marcello,[66A,66C] Z.X. Meng,[57] J.G. Messchendorp,[55] G. Mezzadri,[24A] T.J. Min,[35] R.E. Mitchell,[22] X.H. Mo,[1,49,54] Y.J. Mo,[6] N. Yu. Muchnoi,[10,c] H. Muramatsu,[59] S. Nakhoul,[11,f] Y. Nefedov,[29] F. Nerling,[11,f] I.B. Nikolaev,[10,c] Z. Ning,[1,49] S. Nisar,[8,i] S.L. Olsen,[54] Q. Ouyang,[1,49,54] S. Pacetti,[23B,23C] X. Pan,[9,h] Y. Pan,[58] A. Pathak,[1] P. Patteri,[23A] M. Pelizaeus,[4] H.P. Peng,[63,49] K. Peters,[11,f] J. Pettersson,[67] J.L. Ping,[34] R.G. Ping,[1,54] S. Pogodin,[29] R. Poling,[59] V. Prasad,[63,49] H. Qi,[63,49] H.R. Qi,[52] K.H. Qi,[25] M. Qi,[35] T.Y. Qi,[9] S. Qian,[1,49] W.B. Qian,[54] Z. Qian,[50] C.F. Qiao,[54] L.Q. Qin,[12] X.P. Qin,[9,h] X.S. Qin,[41] Z.H. Qin,[1,49] J.F. Qiu,[1] S.Q. Qu,[36] K.H. Rashid,[65] K. Ravindran,[21] C.F. Redmer,[28] A. Rivetti,[66C] V. Rodin,[55] M. Rolo,[66C] G. Rong,[1,54] Ch. Rosner,[15] M. Rump,[60] H.S. Sang,[63]

JHEP10(2021)177

A. Sarantsev,[29,d] Y. Schelhaas,[28] C. Schnier,[4] K. Schoenning,[67] M. Scodeggio,[24A,24B] D.C. Shan,[46] W. Shan,[19] X.Y. Shan,[63,49] J.F. Shangguan,[46] M. Shao,[63,49] C.P. Shen,[9] H.F. Shen,[1,54] P.X. Shen,[36] X.Y. Shen,[1,54] H.C. Shi,[63,49] R.S. Shi,[1,54] X. Shi,[1,49] X.D. Shi,[63,49] J.J. Song,[41] W.M. Song,[27,1] Y.X. Song,[38,j] S. Sosio,[66A,66C] S. Spataro,[66A,66C] K.X. Su,[68] P.P. Su,[46] F.F. Sui,[41] G.X. Sun,[1] H.K. Sun,[1] J.F. Sun,[16] L. Sun,[68] S.S. Sun,[1,54] T. Sun,[1,54] W.Y. Sun,[34] W.Y. Sun,[27] X. Sun,[20,k] Y.J. Sun,[63,49] Y.K. Sun,[63,49] Y.Z. Sun,[1] Z.T. Sun,[1] Y.H. Tan,[68] Y.X. Tan,[63,49] C.J. Tang,[45] G.Y. Tang,[1] J. Tang,[50] J.X. Teng,[63,49] V. Thoren,[67] W.H. Tian,[43] Y.T. Tian,[25] I. Uman,[53B] B. Wang,[1] C.W. Wang,[35] D.Y. Wang,[38,j] H.J. Wang,[31,m,n] H.P. Wang,[1,54] K. Wang,[1,49] L.L. Wang,[1] M. Wang,[41] M.Z. Wang,[38,j] Meng Wang,[1,54] W. Wang,[50] W.H. Wang,[68] W.P. Wang,[63,49] X. Wang,[38,j] X.F. Wang,[31,m,n] X.L. Wang,[9,h] Y. Wang,[50] Y. Wang,[63,49] Y.D. Wang,[37] Y.F. Wang,[1,49,54] Y.Q. Wang,[1] Y.Y. Wang,[31,m,n] Z. Wang,[1,49] Z.Y. Wang,[1] Ziyi Wang,[54] Zongyuan Wang,[1,54] D.H. Wei,[12] F. Weidner,[60] S.P. Wen,[1] D.J. White,[58] U. Wiedner,[4] G. Wilkinson,[61] M. Wolke,[67] L. Wollenberg,[4] J.F. Wu,[1,54] L.H. Wu,[1] L.J. Wu,[1,54] X. Wu,[9,h] Z. Wu,[1,49] L. Xia,[63,49] H. Xiao,[9,h] S.Y. Xiao,[1] Z.J. Xiao,[34] X.H. Xie,[38,j] Y.G. Xie,[1,49] Y.H. Xie,[6] T.Y. Xing,[1,54] G.F. Xu,[1] Q.J. Xu,[14] W. Xu,[1,54] X.P. Xu,[46] Y.C. Xu,[54] F. Yan,[9,h] L. Yan,[9,h] W.B. Yan,[63,49] W.C. Yan,[71] Xu Yan,[46] H.J. Yang,[42,g] H.X. Yang,[1] L. Yang,[43] S.L. Yang,[54] Y.X. Yang,[12] Yifan Yang,[1,54] Zhi Yang,[25] M. Ye,[1,49] M.H. Ye,[7] J.H. Yin,[1] Z.Y. You,[50] B.X. Yu,[1,49,54] C.X. Yu,[36] G. Yu,[1,54] J.S. Yu,[20,k] T. Yu,[64] C.Z. Yuan,[1,54] L. Yuan,[2] X.Q. Yuan,[38,j] Y. Yuan,[1] Z.Y. Yuan,[50] C.X. Yue,[32] A. Yuncu,[53A,a] A.A. Zafar,[65] Zeng,[6] Y. Zeng,[20,k] A.Q. Zhang,[1] B.X. Zhang,[1] Guangyi Zhang,[16] H. Zhang,[63] H.H. Zhang,[27] H.H. Zhang,[50] H.Y. Zhang,[1,49] J.J. Zhang,[43] J.L. Zhang,[69] J.Q. Zhang,[34] J.W. Zhang,[1,49,54] J.Y. Zhang,[1] J.Z. Zhang,[1,54] Jianyu Zhang,[1,54] Jiawei Zhang,[1,54] L.M. Zhang,[52] L.Q. Zhang,[50] Lei Zhang,[35] S. Zhang,[50] S.F. Zhang,[35] Shulei Zhang,[20,k] X.D. Zhang,[37] X.Y. Zhang,[41] Y. Zhang,[61] Y.H. Zhang,[1,49] Y.T. Zhang,[63,49] Yan Zhang,[63,49] Yao Zhang,[1] Z.H. Zhang,[6] Z.Y. Zhang,[68] G. Zhao,[1] J. Zhao,[32] J.Y. Zhao,[1,54] J.Z. Zhao,[1,49] Lei Zhao,[63,49] Ling Zhao,[1] M.G. Zhao,[36] Q. Zhao,[1] S.J. Zhao,[71] Y.B. Zhao,[1,49] Y.X. Zhao,[25] Z.G. Zhao,[63,49] A. Zhemchugov,[29,b] B. Zheng,[64] J.P. Zheng,[1,49] Y. Zheng,[38,j] Y.H. Zheng,[54] B. Zhong,[34] C. Zhong,[64] L.P. Zhou,[1,54] Q. Zhou,[1,54] X. Zhou,[68] X.K. Zhou,[54] X.R. Zhou,[63,49] X.Y. Zhou,[32] A.N. Zhu,[1,54] J. Zhu,[36] K. Zhu,[1] K.J. Zhu,[1,49,54] S.H. Zhu,[62] T.J. Zhu,[69] W.J. Zhu,[9,h] W.J. Zhu,[36] Y.C. Zhu,[63,49] Z.A. Zhu,[1,54] B.S. Zou[1] and J.H. Zou[1]

[1] *Institute of High Energy Physics, Beijing 100049, People's Republic of China*
[2] *Beihang University, Beijing 100191, People's Republic of China*
[3] *Beijing Institute of Petrochemical Technology, Beijing 102617, People's Republic of China*
[4] *Bochum Ruhr-University, D-44780 Bochum, Germany*
[5] *Carnegie Mellon University, Pittsburgh, Pennsylvania 15213, USA*
[6] *Central China Normal University, Wuhan 430079, People's Republic of China*
[7] *China Center of Advanced Science and Technology, Beijing 100190, People's Republic of China*
[8] *COMSATS University Islamabad, Lahore Campus, Defence Road, Off Raiwind Road, 54000 Lahore, Pakistan*
[9] *Fudan University, Shanghai 200443, People's Republic of China*
[10] *G.I. Budker Institute of Nuclear Physics SB RAS (BINP), Novosibirsk 630090, Russia*
[11] *GSI Helmholtzcentre for Heavy Ion Research GmbH, D-64291 Darmstadt, Germany*
[12] *Guangxi Normal University, Guilin 541004, People's Republic of China*
[13] *Guangxi University, Nanning 530004, People's Republic of China*
[14] *Hangzhou Normal University, Hangzhou 310036, People's Republic of China*
[15] *Helmholtz Institute Mainz, Staudinger Weg 18, D-55099 Mainz, Germany*
[16] *Henan Normal University, Xinxiang 453007, People's Republic of China*
[17] *Henan University of Science and Technology, Luoyang 471003, People's Republic of China*
[18] *Huangshan College, Huangshan 245000, People's Republic of China*

JHEP10(2021)177

[19] Hunan Normal University, Changsha 410081, People's Republic of China
[20] Hunan University, Changsha 410082, People's Republic of China
[21] Indian Institute of Technology Madras, Chennai 600036, India
[22] Indiana University, Bloomington, Indiana 47405, USA
[23] INFN Laboratori Nazionali di Frascati , (A)INFN Laboratori Nazionali di Frascati, I-00044, Frascati, Italy; (B)INFN Sezione di Perugia, I-06100, Perugia, Italy; (C)University of Perugia, I-06100, Perugia, Italy
[24] INFN Sezione di Ferrara, (A)INFN Sezione di Ferrara, I-44122, Ferrara, Italy; (B)University of Ferrara, I-44122, Ferrara, Italy
[25] Institute of Modern Physics, Lanzhou 730000, People's Republic of China
[26] Institute of Physics and Technology, Peace Ave. 54B, Ulaanbaatar 13330, Mongolia
[27] Jilin University, Changchun 130012, People's Republic of China
[28] Johannes Gutenberg University of Mainz, Johann-Joachim-Becher-Weg 45, D-55099 Mainz, Germany
[29] Joint Institute for Nuclear Research, 141980 Dubna, Moscow region, Russia
[30] Justus-Liebig-Universitaet Giessen, II. Physikalisches Institut, Heinrich-Buff-Ring 16, D-35392 Giessen, Germany
[31] Lanzhou University, Lanzhou 730000, People's Republic of China
[32] Liaoning Normal University, Dalian 116029, People's Republic of China
[33] Liaoning University, Shenyang 110036, People's Republic of China
[34] Nanjing Normal University, Nanjing 210023, People's Republic of China
[35] Nanjing University, Nanjing 210093, People's Republic of China
[36] Nankai University, Tianjin 300071, People's Republic of China
[37] North China Electric Power University, Beijing 102206, People's Republic of China
[38] Peking University, Beijing 100871, People's Republic of China
[39] Qufu Normal University, Qufu 273165, People's Republic of China
[40] Shandong Normal University, Jinan 250014, People's Republic of China
[41] Shandong University, Jinan 250100, People's Republic of China
[42] Shanghai Jiao Tong University, Shanghai 200240, People's Republic of China
[43] Shanxi Normal University, Linfen 041004, People's Republic of China
[44] Shanxi University, Taiyuan 030006, People's Republic of China
[45] Sichuan University, Chengdu 610064, People's Republic of China
[46] Soochow University, Suzhou 215006, People's Republic of China
[47] South China Normal University, Guangzhou 510006, People's Republic of China
[48] Southeast University, Nanjing 211100, People's Republic of China
[49] State Key Laboratory of Particle Detection and Electronics, Beijing 100049, Hefei 230026, People's Republic of China
[50] Sun Yat-Sen University, Guangzhou 510275, People's Republic of China
[51] Suranaree University of Technology, University Avenue 111, Nakhon Ratchasima 30000, Thailand
[52] Tsinghua University, Beijing 100084, People's Republic of China
[53] Turkish Accelerator Center Particle Factory Group, (A)Istanbul Bilgi University, 34060 Eyup, Istanbul, Turkey; (B)Near East University, Nicosia, North Cyprus, Mersin 10, Turkey
[54] University of Chinese Academy of Sciences, Beijing 100049, People's Republic of China
[55] University of Groningen, NL-9747 AA Groningen, The Netherlands
[56] University of Hawaii, Honolulu, Hawaii 96822, USA
[57] University of Jinan, Jinan 250022, People's Republic of China
[58] University of Manchester, Oxford Road, Manchester, M13 9PL, United Kingdom
[59] University of Minnesota, Minneapolis, Minnesota 55455, USA
[60] University of Muenster, Wilhelm-Klemm-Str. 9, 48149 Muenster, Germany
[61] University of Oxford, Keble Rd, Oxford, UK OX13RH
[62] University of Science and Technology Liaoning, Anshan 114051, People's Republic of China
[63] University of Science and Technology of China, Hefei 230026, People's Republic of China

JHEP10(2021)177

[64] University of South China, Hengyang 421001, People's Republic of China
[65] University of the Punjab, Lahore-54590, Pakistan
[66] University of Turin and INFN, (A)University of Turin, I-10125, Turin, Italy; (B)University of Eastern Piedmont, I-15121, Alessandria, Italy; (C)INFN, I-10125, Turin, Italy
[67] Uppsala University, Box 516, SE-75120 Uppsala, Sweden
[68] Wuhan University, Wuhan 430072, People's Republic of China
[69] Xinyang Normal University, Xinyang 464000, People's Republic of China
[70] Zhejiang University, Hangzhou 310027, People's Republic of China
[71] Zhengzhou University, Zhengzhou 450001, People's Republic of China

[a] Also at Bogazici University, 34342 Istanbul, Turkey
[b] Also at the Moscow Institute of Physics and Technology, Moscow 141700, Russia
[c] Also at the Novosibirsk State University, Novosibirsk, 630090, Russia
[d] Also at the NRC "Kurchatov Institute", PNPI, 188300, Gatchina, Russia
[e] Also at Istanbul Arel University, 34295 Istanbul, Turkey
[f] Also at Goethe University Frankfurt, 60323 Frankfurt am Main, Germany
[g] Also at Key Laboratory for Particle Physics, Astrophysics and Cosmology, Ministry of Education; Shanghai Key Laboratory for Particle Physics and Cosmology; Institute of Nuclear and Particle Physics, Shanghai 200240, People's Republic of China
[h] Also at Key Laboratory of Nuclear Physics and Ion-beam Application (MOE) and Institute of Modern Physics, Fudan University, Shanghai 200443, People's Republic of China
[i] Also at Harvard University, Department of Physics, Cambridge, MA, 02138, USA
[j] Also at State Key Laboratory of Nuclear Physics and Technology, Peking University, Beijing 100871, People's Republic of China
[k] Also at School of Physics and Electronics, Hunan University, Changsha 410082, China
[l] Also at Guangdong Provincial Key Laboratory of Nuclear Science, Institute of Quantum Matter, South China Normal University, Guangzhou 510006, China
[m] Also at Frontiers Science Center for Rare Isotopes, Lanzhou University, Lanzhou 730000, People's Republic of China
[n] Also at Lanzhou Center for Theoretical Physics, Lanzhou University, Lanzhou 730000, People's Republic of China

JHEP10(2021)177